

Multiscale patterns of migration flows in Austria: regionalization, administrative barriers, and urban-rural divides

Thomas Robiglio^{1,2,*}, Martina Contisciani^{2,*}, Márton Karsai^{2,3}, and Tiago P. Peixoto^{1,2}

¹Inverse Complexity Lab, IT:U Interdisciplinary Transformation University Austria, 4040 Linz, Austria

²Department of Network and Data Science, Central European University, 1100 Vienna, Austria

³National Laboratory for Health Security, HUN-REN Alfréd Rényi Institute of Mathematics, Budapest, 1053, Hungary

*These authors contributed equally to this work

Abstract

Migration is central in various societal problems related to socioeconomic development. While much of the existing research has focused on international migration, migration patterns within a single country remain relatively unexplored. In this work we study internal migration patterns in Austria for a period of over 20 years, obtained from open and high-granularity administrative records. We employ inferential network methods to characterize the flows between municipalities and extract their clustering according to similar target and destination rates. Our methodology reveals significant deviations from commonly assumed relocation patterns modeled by the gravity law. At the same time, we observe unexpected biases of internal migrations that leads to less frequent movements across boundaries at both district and state levels than predictions suggest. This leads to significant regionalization of migration at multiple geographical scales and augmented division between urban and rural areas. These patterns appear to be remarkably persistent across decades of migration data, demonstrating systematic limitations of conventionally used gravity models in migration studies. Our approach presents a robust methodology that can be used to improve such evaluations, and can reveal new phenomena in migration networks.

I. Introduction

Migration plays a central role in urbanization, segregation, gentrification, and in many phenomena related to socioeconomic development [1]. The driving forces of migration can be extremely varied, including labor market imbalances, wealth inequalities, conflicts, ethnoracial segregation—reflecting the rapid increase in complexity of human societies [2]. Migration has increasingly become a crucial topic in public discourse and in regional and national governance, drawing considerable attention in academic research. In recent years, researchers from various fields have investigated why people migrate, how migration takes place, and what the consequences of migration are in a broad sense, both for the migrants themselves and for the communities involved [3]. However, much of this research has mainly focused on international migration, leaving many questions unanswered for a comprehensive understanding of internal (or domestic) migration. Since the majority of migration events in the world occur within national borders, an emphasis on international migrations overlooks a significant portion of the overall migration phenomenon. Additionally, focusing on international migrations restricts our ability to fully assess social dynamics and the impacts of policy interventions at the local level. To address these gaps, we analyze internal migration data from Austria spanning a 20-year period, providing a mesoscopic analysis of domestic relocation patterns.

A common approach for analyzing migration data—and human mobility in general—is to develop statistical models that allow researchers to uncover the underlying forces driving these phenomena, make predictions, and test hypotheses [4]. At an individual level, these include random walk frameworks to characterize mobility trajectories [5–7]. At a population level, the usual task is to model collective flows between locations, based on attributes such as population densities, geographic distance, and socio-economic indicators. The most commonly used modeling ansatz for this purpose is based on the pervasive empirical observation that the rate of movement between two regions tends to increase according to the product of their population densities, and inversely proportional to a function of their distance [8], which leads to a family of so-called “gravity” models [9–11], due the functional similarity with Newton’s law of gravitation. This pattern is observed in many different kinds of mobility and human behavior, including commutes [12, 13], daily movements [14, 15], mobile phone communications [16], and migration [8, 17]. The simple form of this model family allows for an

intuitive interpretation in terms of the overall attractivity of each region, which is reasonably correlated to its population, and the cost of movement, which should grow with distance. However, the precise functional shape of gravity models, and in particular their parameters, are not derived from first principles, or from more fundamental processes of mobility, rendering them effective, rather than mechanistic in nature. Important alternatives to gravity models do exist, which attempt to include more mechanistic elements, such as the “intervening opportunities” model [18, 19], which discards the explicit dependence on distance, in favor of the cumulative number of “opportunities” between source and destination, which although it typically increases with distance, it can also be associated with other factors. Another, more recent alternative is the radiation model [20], which posits, similarly, that a traveler ranks the available opportunities according to their distance, and chooses the closest one above a certain fitness threshold. In general, however, most available empirical mobility data do not offer more statistical evidence for these alternative models when compared to the gravity ansatz, which often has a better quality of fit and is more predictive [12, 21], although not by large margins.

Due to the effective and heuristic nature of gravity models, they are not expected to saturate the modeling requirements of mobility data, and in fact many systematic deviations have been observed in previous studies, such as the inability to model behaviors for long distances [20–22], and the overdispersion commonly seen in the data [23–25], when compared to model predictions.

In this work, we are interested in further modeling migration dynamics and evaluating the gravity model, but from the point of view of arbitrary geographic discrepancies that are not *a priori* posited explicitly, but instead are discovered *a posteriori* from data. We do so by leveraging an inferential network clustering method [26, 27], that fits a nonparametric generative model to empirical data, instead of enforcing a particular functional shape for the migration rates. Our model approximates any functional shape by separating the regions into discrete groups, and therefore their corresponding migration rates as piecewise mixtures of elementary distributions. Our procedure includes Bayesian regularization based on the minimum description length principle [28, 29], and hence is robust against overfitting. In addition, our model works in a hierarchical fashion [30], so that the mixing patterns between geographical regions are simultaneously modeled at multiple scales.

Based on this inferential analysis, we compare the properties of the inferred nonparametric and multiscale model to a fitted gravity model, which then allows us to identify statistically significant discrepancies.

When applying our method to internal migration data for Austria, interestingly, we find systematic biases in migration flows where administrative boundaries appear as effective barriers for relocation. These biases lead to clusters in the migration network that resemble administrative borders between federal states and districts with a remarkable accuracy. This indicates a reduced importance of distance in determining internal migration events, in addition to strong regionalization and elevated urban-rural divide as compared to gravity model predictions.

II. Results

Our analysis examines the network of internal migration in Austria in the period from 2002 to 2021, where each node represents a municipality, and each directed edge denotes the number of individuals relocating from one municipality to another. We aggregate the data annually and analyze twenty distinct networks that capture migration flows for each year. Alternatively, one could consider combining all data into a single aggregated network. However, such an approach would hinder our ability to evaluate the consistency of migration patterns and the robustness of our findings over time. Additional information on the data, such as the number of nodes and edges for each year, is provided in Sec. IV.

Similarly to what is observed in a variety of other mobility data, migration flows between two locations tend to decay with the distance between them, and increase with the population densities of the source and target of the migration—presumably due to the increased cost of farther relocations, and the opportunities associated with moving to higher population areas. This is typically modeled via a gravity model, where the

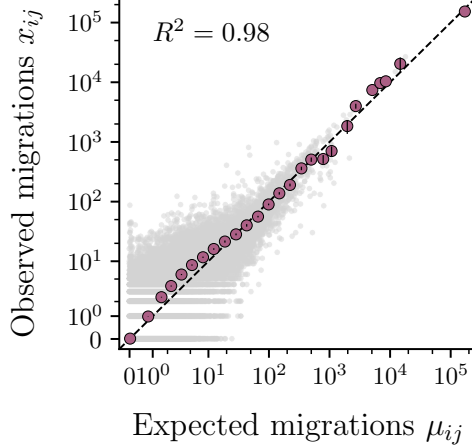


Figure 1: Observed migration counts x_{ij} versus expected counts μ_{ij} according to the inferred gravity model, between municipalities in Austria in 2013. The red circles show average values for equal sized bins, along with their standard error. The dashed line represents the $x_{ij} = \mu_{ij}$ diagonal slope. The coefficient of determination R^2 is shown for the fitted model.

expected number of migrations x_{ij} from locations j to i is given by

$$\langle x_{ij} \rangle = \mu_{ij} = K \frac{(p_i p_j)^\alpha}{d_{ij}^\beta}, \quad (1)$$

where p_i is the population of location i , and d_{ij} is the distance between locations i and j . The remaining parameters K , α , and β are to be inferred from data, since they are context-dependent. We use a Bayesian approach to infer the unknown parameters by sampling from their joint posterior distribution using Hamiltonian Monte Carlo [31, 32]. For further details, we refer to Sec. V.

In Fig. 1 we show a comparison between the observed and expected migration counts between municipalities in Austria in 2013, according to the inferred gravity model. From this type of analysis, which is typically performed in mobility studies, one could conclude that the gravity model offers a fairly good fit to the data, with the only noticeable deviation being a systematic discrepancy for low values of μ_{ij} in the range between 3 to 20 (corresponding to movements between large distances and/or low populations areas), where more migration events are observed than would be expected by the gravity model. Already anticipating one of our results obtained via nonparametric inference, further insight into this discrepancy can be obtained by stratifying the migrations in two groups, according to whether or not an administrative boundary has been crossed. In Fig. 2 we show this stratification according to the boundaries between district and federal states. In both cases we see that the discrepancies for low μ_{ij} values are exacerbated within administrative boundaries (Fig. 2a and c), and vanish when these are crossed (Fig. 2b and d). Instead, in the latter case, deviations for high μ_{ij} are seen (i.e. between short distances and/or high population areas), where the observed migrations are fewer than expected according to the gravity ansatz.

If the gravity model would hold uniformly for all migrations between municipalities, this discrepancy would not be expected. However, since the model is based on a very specific relationship between distance and population, it is difficult to interpret these deviations, since not only these two quantities cannot be disentangled, but also the model is incapable of incorporating other types of geographic dependencies.

To better understand the deviations from the gravity model, we relax the assumptions of Eq. (1), and consider instead a more general model based on a weighted stochastic block model (WSBM) formulation [27]. More specifically, given a partition \mathbf{b} of the municipalities into B groups, where $b_i \in \{0, \dots, B-1\}$ is the group

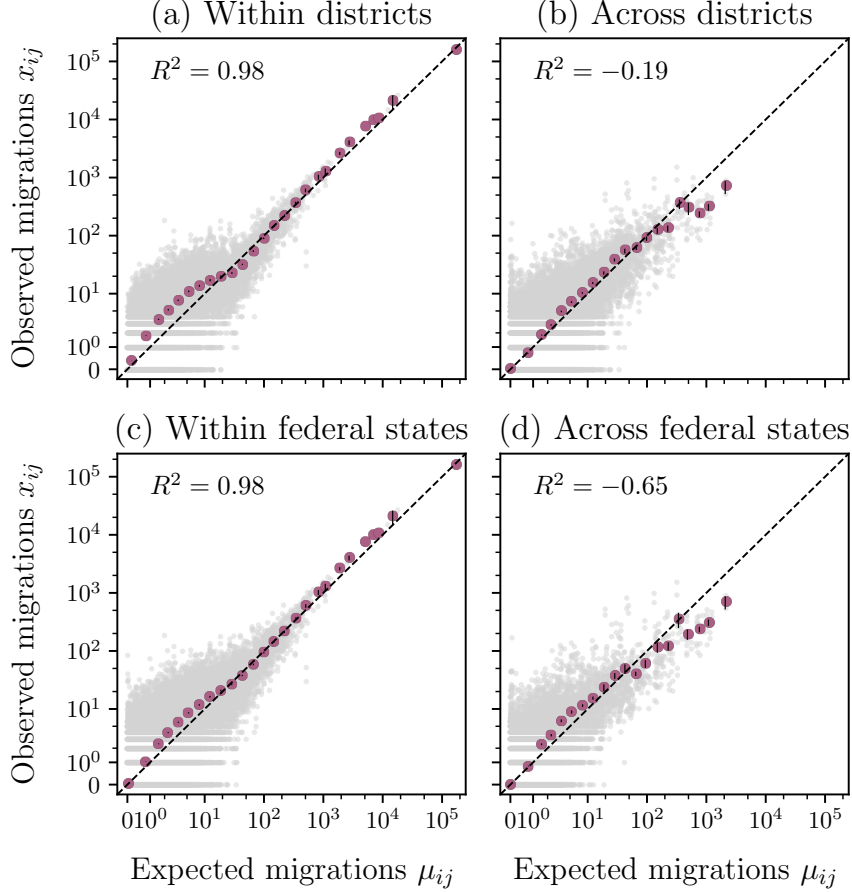


Figure 2: Same analysis of Fig. 1, but containing only migrations within a single administrative region (left panels) and across two or more (right panels). The top panels consider districts, and the bottom panels federal states. The expected migrations are inferred from the entire data (i.e., the same as in Fig. 1), and therefore are the same for all panels, instead of being fitted individually. Likewise, the coefficient of determination R^2 for each panel is calculated with respect to the same overall model fitted on the whole data. Hence, a negative value is possible, and indicates a situation where the mean of the data provides a better fit than the function considered.

membership of municipality i , we model the number of migrations between municipalities according to

$$P(\mathbf{x}|\boldsymbol{\theta}, \mathbf{b}) = \prod_{ij} P(x_{ij}|\theta_{b_i, b_j}), \quad (2)$$

where $P(x|\theta_{r,s})$ is a kernel distribution (e.g. Poisson or geometric) with parameters $\theta_{r,s}$ that are conditioned only the groups r and s of the edge endpoints. Therefore, by choosing this kernel distribution, the number of groups, and how the nodes are partitioned into it, we can approximate a wide variety of distributions, including those that deviate significantly from the gravity model. Importantly, we do not require the municipalities to be grouped in spatially contiguous regions, and do not enforce any dependency of the migration rates with distance or population. If such dependencies actually do exist in the data, we should be able to detect them, but we allow for any mixing pattern between groups of municipalities to be uncovered as well. This can be contrasted with most descriptive community detection methods [33], which not only expect and enforce a larger number of connections between nodes of the same group than otherwise (independently of whether this is the most salient or even statistically valid pattern in the data [34]), but they are also unaffected by mixing preferences between nodes of different groups.

In order to perform the inference of the model of Eq. (2), we employ the Bayesian approach described in Ref. [27], which determines the most appropriate model according to the minimum description length (MDL) principle [28, 29], that provides robustness against overfitting. One important aspect of our method is that it yields a hierarchical partition, i.e. the groups themselves are clustered into their own groups, and so on recursively, yielding a description of the data in multiple scales. For further details on the methodology, we refer to Sec. V.

In Fig. 3a we show the hierarchical partition of the internal migration network in 2013, which reveals a heterogeneous group structure, largely aligned with wider geographical regions at the upper levels. We emphasize that our model does not *a priori* enforce or expect this pattern, and the fact it is found means migration is strongly regionalized, both at a local and global scales. The migration volumes between municipalities vary by several orders of magnitude, with intra-municipality relocations (i.e., self-loops in Fig. 3a, or the diagonal entries in 3b) being the most numerous, with a migration rate that increases with the respective populations. This observation is compatible with the gravity model ansatz, since these are the relocations with the shortest distances, and also between the largest population densities in the case of some municipalities.

However, what is well captured by our WSBM, but not so much by the gravity model, is the strength and specificity of the regionalization, with the overall regions and federal states being very well captured by the hierarchical partition. This becomes especially evident when the inferred partitions are overlaid on the map of Austria, as shown in Fig. 4. Furthermore, the lowest inferred hierarchical level (Fig. 4a) also separates the larger cities and urban areas from the rest, which act as source and destination hubs for migrations to and from both large and small municipalities, as well as nearby and distant locations. This is more clearly illustrated in Fig. 3b, where the communities containing Wien, Graz, and Salzburg (respectively, communities 0, 1, and 39, at level $l = 0$) show large out-diagonal entries, indicating frequent interactions with all other communities. Additionally, this plot highlights that the overall mixing pattern is highly assortative at all levels, meaning that individuals are more likely to migrate within the same cluster, and the same sub-cluster inside that cluster, which often corresponds to a specific geographical region.

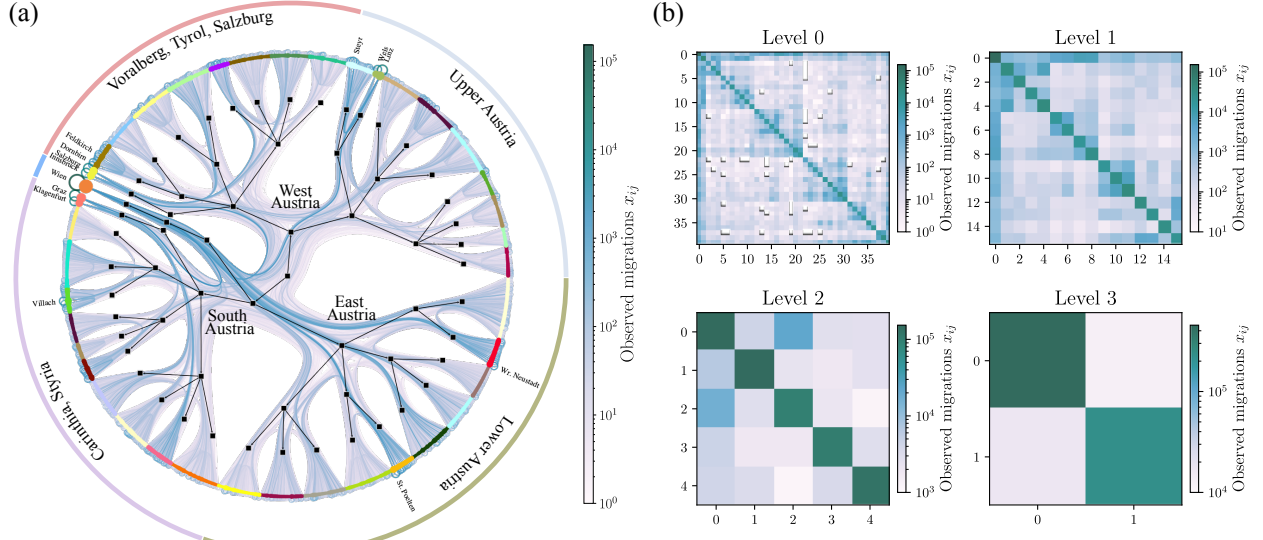
In the bottom panels of Fig. 3 we show also the deviation of the observed flows between groups from what would be expected with the gravity model, via the z-score between groups r and s defined as

$$z_{rs} = \frac{x_{rs} - \mu_{rs}}{\sqrt{\mu_{rs}}}, \quad (3)$$

where $x_{rs} = \sum_{ij} x_{ij} \delta_{b_i, r} \delta_{b_j, s}$ and $\mu_{rs} = \sum_{ij} \mu_{ij} \delta_{b_i, r} \delta_{b_j, s}$, and we used the fact that the sum of independent Poisson variables is also Poisson-distributed with the summed means. A positive or negative value with magnitude $|z_{rs}| > 3$ is considered significant, and means that the gravity model formulation cannot plausibly account for the deviation. Specifically, positive z-scores (shown in blue) imply that the observed migrations exceed the model's expectations—i.e., the gravity model underestimates the flows. Conversely, negative values (shown in red) indicate an overestimation by the model. As we see in Fig. 3c, relative to the gravity model, there are fewer migration events between many nearby regions of Lower Austria and Vienna, which is compensated for a relative abundance of migrations from farther regions in Vorarlberg, Tyrol, and Salzburg. Most internal migrations between inferred clusters tend to exceed the expectation from the gravity model, with a few exceptions where the opposite is observed.

What is perhaps the most striking feature of this inferred regionalization is how well it aligns with administrative boundaries. In Fig. 5a and b we show the overlap between districts and federal states with the boundaries between the inferred groups, which show a remarkable agreement: Around 45% of the district boundaries coincide exactly with the boundaries between the inferred groups, and the same happens for around 72% of the federal state boundaries. The overlap becomes even more pronounced once we perform the same inference for a binarized version of the network, where we ignore the magnitude of migrations, and consider instead a simple directed graph, where an edge exists between two municipalities if any non-zero number of migrations have occurred between them. In this case, the percentage of administrative regions that match the inferred divisions increases to 78% and 95%, for district and federal state boundaries, respectively. (We emphasize that our inferred clustering is based only on the number of migrations between municipalities, without including any direct geographical information of any kind.) This observation might be counterintuitive, as one could expect that incorporating migration magnitudes would reinforce existing

Migration flows



Deviations from the gravity model

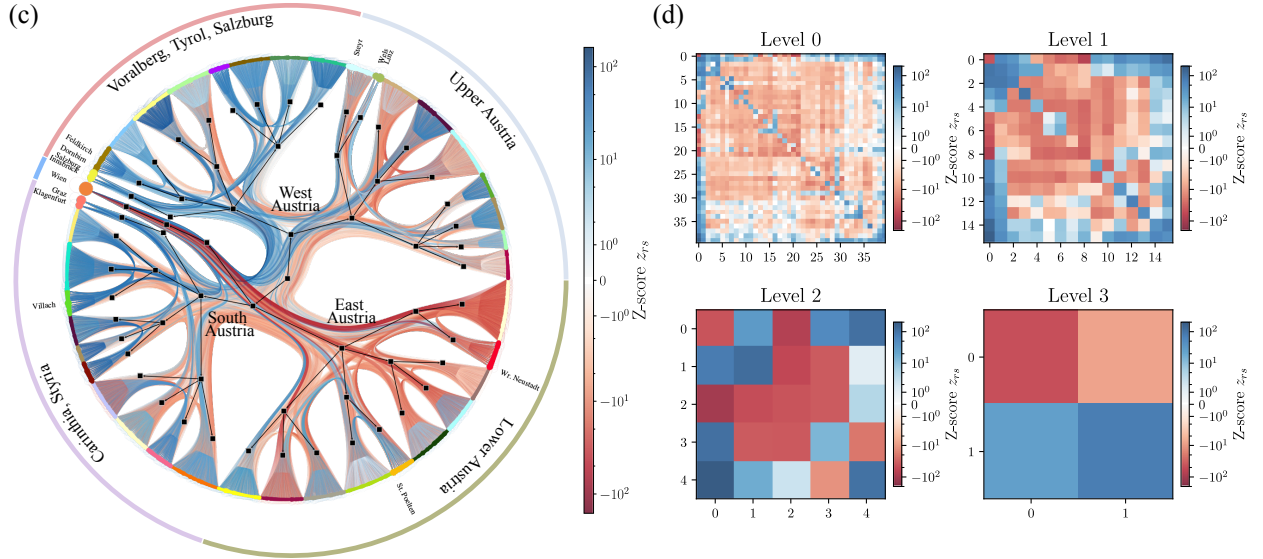
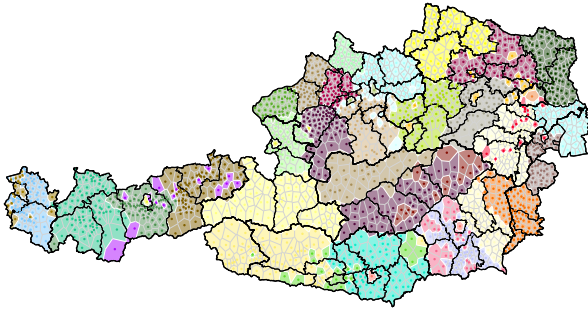
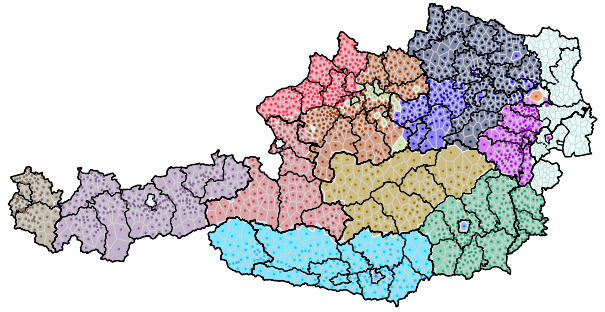


Figure 3: (a) Fit of the WSBM for Austrian migrations in 2013. The edges are routed according to the inferred hierarchy (shown in black), using an edge-bundling layout [35]. The color of the edges indicates their count of migration events in the year. The size of the nodes is proportional to their population. The color of the nodes corresponds to the partition they belong to at hierarchical level $l = 0$. The partitions at level $l = 2$ are shown with the outer circular arcs. Cities names are shown for the 13 largest cities. Levels 2 and 3 are annotated with the most frequent federal state classifications (NUTS2), and general areas (NUTS1), respectively. (b) Corresponding matrices of migration counts between groups for the four different levels of the hierarchy. The bottom panels (c) and (d) correspond to (a) and (b), but they show instead the group-level deviation from the gravity model via the z-score, as defined in Eq. (3). Blue edges indicate positive discrepancies, meaning that more migration events are observed than predicted by the gravity model. Conversely, red edges represent negative deviations, where the observed migrations are fewer than expected.

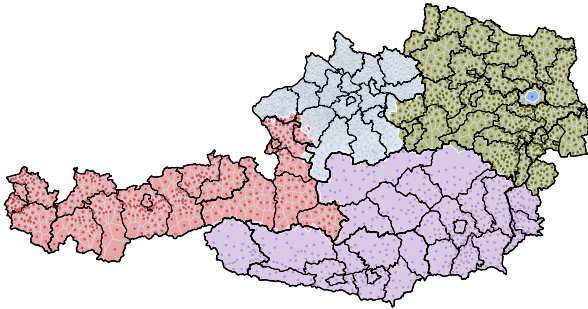
(a) Inferred groups at level $l = 0$



(b) Inferred groups at level $l = 1$



(c) Inferred groups at level $l = 2$



(d) Inferred groups at level $l = 3$

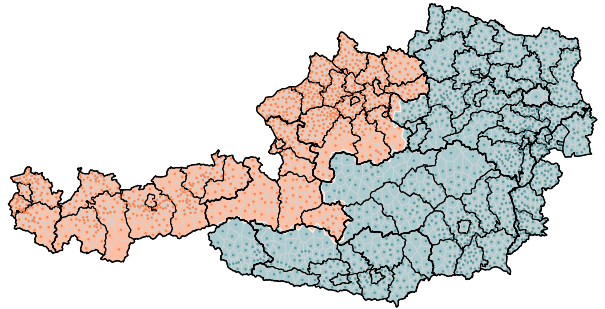
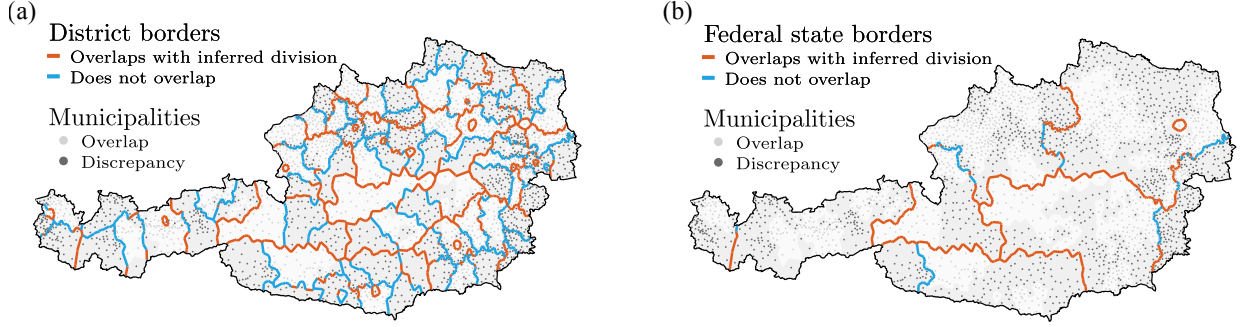


Figure 4: Inferred groups with the WSBM for 2013, for different hierarchical levels l . Thick black lines indicate federal states boundaries, thin black lines denote districts borders.

Full migration network



Binarized network

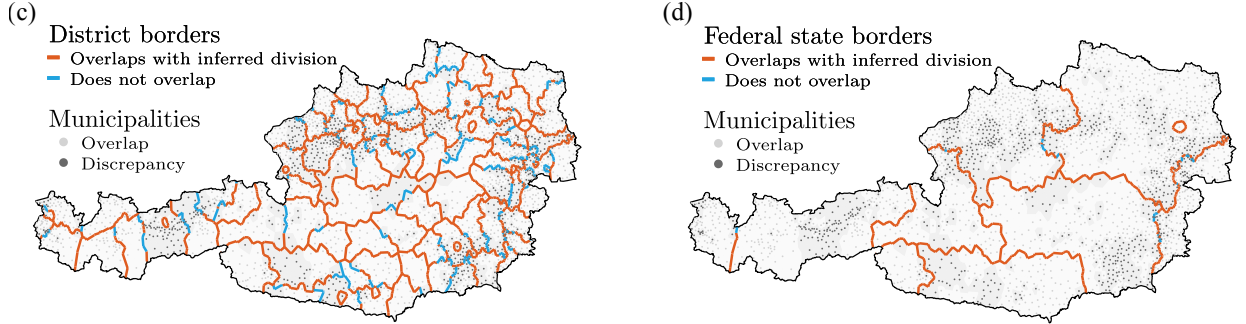


Figure 5: Comparison between administrative borders and the boundaries between groups of the municipalities inferred with the WSBM for 2013. If an administrative border coincides with the inferred partition, it is shown in red, otherwise in blue. Dark gray nodes indicate areas of discrepancy between the districts and the inferred partition at level $l = 0$. Panel (a) shows how the borders between districts are recovered by the inferred divisions, corresponding to a recall of 0.47, and (b) with the federal states, where the recall increases to 0.72. Panels (c) and (d) show the same as (a) and (b), respectively, but for a binarized network, where an edge either exists or not between two municipalities, depending on whether the migration count is nonzero. In this case, the recall becomes 0.78 and 0.95 for (c) and (d), respectively.

patterns. Instead, including the magnitudes seems to diminish the visibility of district-level effects. This may be because the most substantial migration flows occur between broader regions. This would thereby reduce the relative influence of districts compared to larger administrative divisions such as NUTS1 (general areas) and NUTS2 (federal states), when the migration magnitudes are considered. This result highlights that while administrative boundaries do seem to act as barriers to migration, their influence is not uniform and varies depending on the intensity of the flows. The substantial match between inferred and administrative boundaries is not an exception for the year 2013, and persists instead for the whole 20 years studied, as shown in Fig. 6a. This stability is due to the inferred partitions showing only a small variation over time, as can be seen in the comparison in Fig. 6b, which reveals a very high partition overlap [36] between different times, with only a very tenuous decay for longer time differences.

In addition to the overlap with the boundaries, and groups which are geographically localized, we also observe subdivisions of the administrative districts, as well as groups that are spatially discontinuous and composed of municipalities that are geographically distant. Interestingly, these fragmented communities tend to include more urbanized areas such as large cities. We show this in Fig. 7, which contains the urbanization level of the inferred groups, defined as the urban-rural scores assigned to its constituent municipalities, based on Statistik Austria’s classification [37]: 1 corresponds to urban centers, 2 to regional centers, 3 to rural areas surrounding centers, and 4 to rural areas. To further quantify how this relates to our inferred clustering, we calculate the local disassortativity q_r of group r , defined as the ratio of a group’s off-diagonal interactions to

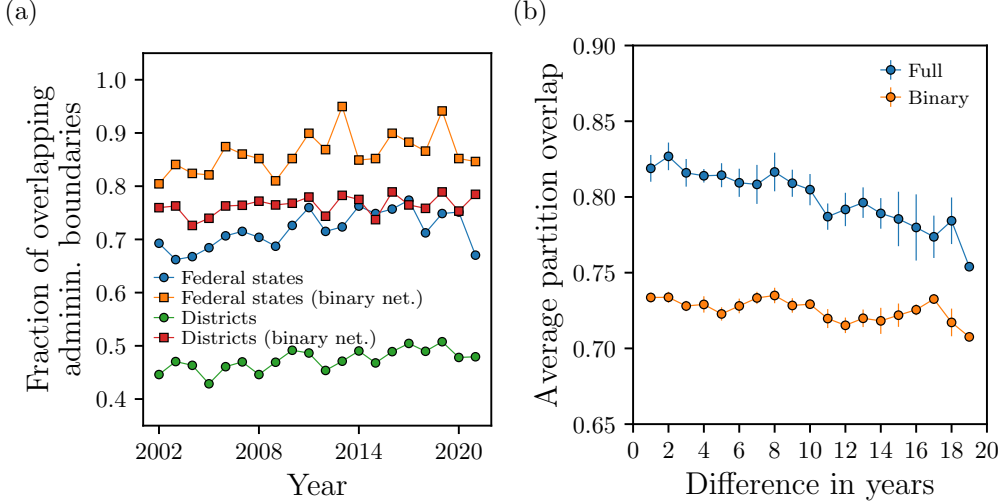


Figure 6: (a) Recall of the administrative boundaries, with respect to the inferred partition, over a span of 20 years, for both districts and federal states, considering both the full network and the binarized version, as shown in the legend. (b) Average overlap between pairs of inferred partitions, as a function of the distance between them in years, both for the full network, as well as the binarized version.

the total off-diagonal entries in the group affinity matrix $\mathbf{m} = \{m_{rs}\}$, where m_{rs} is the number of migrations from group s to group r ,

$$q_r = \frac{\sum_{s:s \neq r} (m_{rs} + m_{sr})}{\sum_{r,s:r \neq s} m_{rs}}. \quad (4)$$

This quantity serves as a proxy of how central a group is, with higher values indicating stronger affinity with a wider variety of groups. Notably, groups with more urbanization (i.e., lower urban-rural score) exhibit greater local disassortativity, suggesting they function as hubs in the migration network. In contrast, rural communities tend to be more self-contained. We quantify this relationship using the Pearson correlation coefficient, which for 2013 is $r = -0.75$, indicating a strong negative correlation between urban-rural level and local disassortativity. These results are consistent across the period from 2002 to 2021, as shown in Fig. 7b.

The observed interaction patterns differ notably from those predicted by the gravity model, as shown in more detail in Figs. 8a and c, where we compare the observed number of migrations across and within administrative boundaries, with the respective expected number according to the best-fitting gravity model. Likewise, in the same figure we do the same comparison with migrations across and inside urban and rural regions. Relative to the gravity model, we observe a stronger tendency for individuals to move within administrative boundaries and a lower frequency of cross-border movements. Significant deviations also emerge when considering the urban-rural classification of the target location. Within administrative boundaries (at the district or federal state level), individuals are more likely to relocate to rural centers and less to urban centers than predicted by the gravity model. Conversely, when crossing administrative borders, there is a pronounced preference for moving to and from urban areas, well above model expectations.

To further detail the discrepancies with the gravity model, we generate 100 synthetic migration data for each year using the best fitting parameters for the data, and apply the WSBM analysis to these artificial samples, as we did with the empirical data. Fig. 8c shows the inferred groups at hierarchical level $l = 0$ for one of the samples, which differ significantly from those identified in the empirical data. In particular, in the synthetic data, the inferred group structures appear to be driven primarily by distance and population effects, showing little alignment with Austria’s regionalization or administrative borders, which in this case become merely incidental. This observation is reinforced by comparing the recall of federal states and districts from the boundaries of the inferred groups (Fig. 8d). A similar deviation is observed with respect to the urban-rural divide: the negative correlation between local disassortativity and urbanization level found in

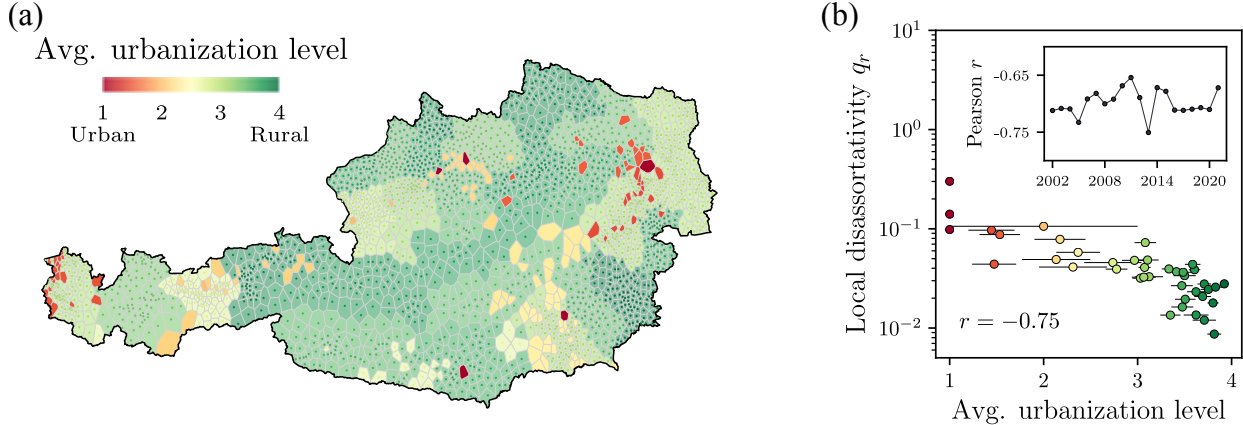


Figure 7: (a) Average urbanization level within the inferred communities at hierarchical level $l = 0$, based on the urban-rural classification from Statistik Austria. (b) Negative correlation between local disassortativity of the communities (as defined in the text) and their urbanization level. Error bars represent the standard error of the urban-rural typology within each inferred group. The inset shows the robustness of this pattern across different years.

the empirical data is much stronger than in the synthetic samples. Taken together, these results show that the gravity model produces samples that fail to replicate key structures and dynamics observed in the real data, highlighting the importance of network inference methods that are more agnostic, and hence are able to uncover meaningful patterns in migration data.

III. Discussion

We have analyzed registry-level data covering all internal migrations in Austria for a period of 20 years, using an inferential clustering methodology that contrasts with the typical approaches used in this context. Such traditional analyses often focus on regression of migration flows with covariates, flow frequency as a function of distance and population density. In contrast, our approach fits an open-ended generative model to the data, which is capable of uncovering statistically significant mixing patterns that do not need to be specifically posited *a priori*. Our method revealed substantial deviations from the gravity model ansatz often used to characterize mobility data, consisting on strong regionalization, a pervasive imprint of administrative boundaries, and an exacerbated urban-rural divide.

The strong correlation of our inferential clustering with administrative boundaries is particularly noteworthy. Similar overlaps with internal administrative boundaries have been observed in other types of human behavior, such as telephone calls in the UK [38], online social networks in the Netherlands [39], geo-tagging trajectories in social media in China [14] and UK [40], bank note circulation in the US [41], daily commutes in Italy [42], and mobile device tracking in China [43] and Hungary [44]. For internal migration in particular, the situation is different: although other studies have performed descriptive clustering analyses for Austria [45], Croatia [46], Turkey [47] and Italy [48], and have also found evidence of regionalization, the precise overlap with administrative boundaries had not yet been quantified.

It is generally expected that administrative boundaries can reflect differences in institutions, public services, and overall economic development [49]. In the case of commuting and daily mobility behavior, as well as migration within the same municipality, it is easy to imagine how administrative demarcations like official zoning, public transport prices, location of schools and public services, and proximity to commercial and/or industrial areas will have a significant impact on how people move or relocate. These movements can then influence local socioeconomic development, real estate prices, crime rates, etc., which in turn can cause changes in the demarcation themselves, and so on. However, in the case of relocation between municipalities and federal states, the precise mechanism that makes administrative boundaries relevant is less clear. Im-

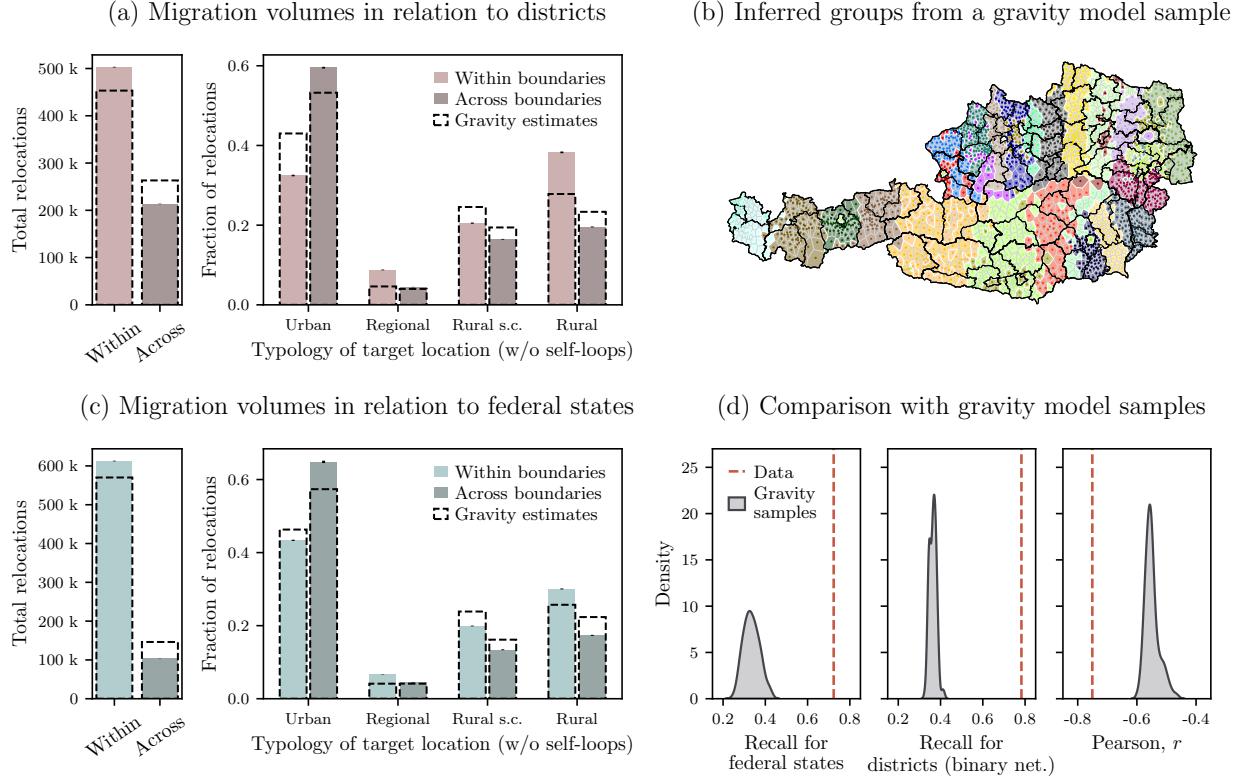


Figure 8: (a) Left: total number of migration events within and across district borders in 2013. Right: fraction of classification of the target location for within and across district boundaries migration events. The dashed bars are the corresponding quantities predicted by the gravity model. (c) Same as above for boundaries between federal states. (b) Groups inferred with the WSBM at hierarchical level $l = 0$ on artificial data sampled from the best-fitting gravity model. (d) Comparison between different descriptors in the data and in samples from the gravity model. Left: recall of the federal state boundaries from the inferred partitions. Center: recall of the district boundaries from the inferred partitions with in the binarized network. Right: Pearson correlation between the local disassortativity and the urbanization level.

portantly, our analysis is not able to determine whether the boundaries act as *causal* barriers for migration, or if the district delineation simply captures the natural ways people would migrate inside the country even if the boundaries would not exist. On the one hand, these internal boundaries have a long history, and capture demographic, cultural, and socio-economical structures of the population that have persisted for a long time. Although the kind of formal municipalities (“Gemeinde”) most comparable to today’s Austria can be traced back to 1849 [50], their *de facto* origin lies often in the middle ages. On the other hand, from the second half of the 20th century, several federal states implemented municipal reforms, often resulting in the merger of municipalities (the latest finalized in the state of Styria in 2015¹, which reduced its number of municipalities from 542 to 287). Some of these merges were reversed decades later, since the local inhabitants felt they did not adequately match the population structures. The actual division of the municipalities into districts (“Bezirke”) stems from 1868, but likewise reflects much older structures, and has also been subject to several reforms in the 20th and 21st centuries, although most of these were rather minor and localized. Our results show that in the 20-year period we analyze, the overlap of our inferred clusters with the administrative boundaries is fairly stable, indicating that the regionalization of internal migration is not deviating significantly.

Regionalization of internal migration had also been previously observed in Austria [45], and other coun-

¹https://www.ris.bka.gv.at/Dokumente/LgblAuth/LGBLA_ST_20140402_31/LGBLA_ST_20140402_31.pdf#sig

	2002	2003	2004	2005	2006	2007	2008	2009	2010	2011
p_{tot}	8063640	8100273	8142573	8201359	8254298	8282984	8307989	8335003	8351643	8375164
E	61829	62152	64194	65404	66150	67565	70203	70372	70830	72412
M	649153	627078	650411	664616	672125	689167	692698	685115	681538	701242

	2012	2013	2014	2015	2016	2017	2018	2019	2020	2021
p_{tot}	8408121	8451860	8507786	8584926	8700471	8772865	8822267	8858775	8901064	8932664
E	72555	73422	74126	78016	80733	78597	78476	78393	78496	78640
M	714697	716436	739918	795028	817139	801624	797666	798420	781472	782995

Table 1: Total population, number of edges in the network, and total number of migration events for each year considered in the dataset. The number of nodes is constant across time and equal to 2093.

tries mentioned previously [46–48], and high urban-rural flows have also been identified in the US [51] and Brazil [52]. However, both of these phenomena can to some extent be associated with the gravity ansatz, since nearby regions are expected to experience higher migration flows, as well as to and from urban centers, which are highly populated. What our analysis shows is that the gravity ansatz coupled with the population distribution of Austria is not sufficient to account for the observed regionalization of migration, and the movements between rural and urban centers.

The residuals of our inferred model with respect to the gravity ansatz revealed a heterogeneous picture, where migrations between regions are either in excess or deficit following a particular pattern. It would be of interest for a future study to correlate such deviations with demographic and socioeconomic indicators, to reveal potential mechanistic explanations. Such explanation could potentially be used to forecast migration, and inform governmental policy.

IV. Data

In this study, we use the publicly available version of the MIGSTAT - WANDERUNGSSTATISTIK dataset [37], which was collected by Statistik Austria, the Federal Statistical Office of Austria. This dataset contains all relocations within Austria that involve a change in main residence under registration law, for the period 2002–2021. We consider each of these change of main residence as a migration event. The data are aggregated at the municipality level (i.e., $N = 2093$), and we analyze each year separately, excluding the information about gender and nationality associated with the relocations.

Our analysis also incorporates the yearly population data (collected at the beginning of each year) of all Austrian municipalities, and the urban-rural typology of these municipalities. Both datasets are provided by Statistik Austria. The urban-rural classification assigns an integer value in the interval $[1, 4]$ to each municipality, with the following mapping: $1 \rightarrow$ urban center, $2 \rightarrow$ regional center, $3 \rightarrow$ rural area surrounding center, and $4 \rightarrow$ rural area. This assignment is produced by integrating information regarding the administrative status of municipalities, the population density across the geographical areas, as well as the infrastructure facilities and the presence of commuting relationships.

A summary of the dataset, with the total population p_{tot} , number of edges E in the network, and total number of migration events M per year is shown in Table 1.

V. Methods

a. Inferring gravity models of migration

Gravity models are among the most widely used tools for analyzing migration and mobility phenomena. The key idea behind these models is that when choosing to migrate, people face the interplay between the cost and the opportunity associated with moving. Typically, the cost of migration is modeled as a function of the distance between the origin and destination of a migration event, while the opportunity is represented

as a function of the product of the population sizes of the two locations. More sophisticated versions of gravity models incorporate additional variables, such as economic or socio-demographic indicators, to better capture the attractiveness of a location or to refine the estimation of moving costs. However, including these additional factors increases the complexity of model and its inference. In this study, we focus on the basic form of the gravity model to allow for clearer interpretation and to draw conclusions from the general formulation, rather than relying on *ad hoc* specifications. In the simple formulation outlined above, the expected amount of migrations x_{ij} from a location j to a location i with population p_j and p_i respectively, and separated by distance d_{ij} , can be expressed as

$$\mu_{ij} = K \frac{(p_i p_j)^\alpha}{d_{ij}^\beta}, \quad (5)$$

where α and β are non-negative real parameters controlling the effect on the population product and distance attributes, while K —also a non-negative real parameter—adjusts the overall magnitude of migration flows.

A common practice in applied research is to take the logarithm of both sides of Eq. (5) and estimate the parameters K , α , and β by finding the best fit of the resulting functional relational form. However, this approach introduces several misspecifications [23], including the treatment of zero values and the biases caused by the logarithmic transformation. Moreover, it overlooks the fact that μ_{ij} in Eq. (5) is a positive real number, while our empirical observations are count values, i.e., non-negative integers. These limitations can be overcome by modeling migration flows between two locations as independent Poisson-distributed random variables, with the expected value (or rate) defined by the functional form of the gravity law [53], i.e.

$$P(\mathbf{x} | K, \alpha, \beta) = \prod_{i,j} \frac{\mu_{ij}^{x_{ij}} e^{-\mu_{ij}}}{x_{ij}!}. \quad (6)$$

To apply the gravity model to the Austrian migration data analyzed in this study, we need to address the presence of intra-municipality migrations, i.e., self-loops in the network with $d_{ij} = 0$. For that, we introduce a specific formulation for the Poisson rate in the case where $i = j$,

$$\mu_{ij} = \begin{cases} K \frac{(p_i p_j)^\alpha}{d_{ij}^\beta} & \text{if } i \neq j \\ C p_i^\delta & \text{if } i = j \end{cases} \quad (7)$$

where C and δ are non-negative real parameters independently capturing intra-municipality migration dynamics. Based on this formulation, the model parameters $(K, \alpha, \beta, C, \delta)$ are inferred from data on migration counts \mathbf{x} according to the joint posterior distribution

$$P(K, \alpha, \beta, C, \delta | \mathbf{x}) = \frac{P(\mathbf{x} | K, \alpha, \beta, C, \delta) P(K, \alpha, \beta, C, \delta)}{P(\mathbf{x})}, \quad (8)$$

with $P(K, \alpha, \beta, C, \delta) \propto 1$ being a noninformative prior. Samples from this posterior distribution are obtained using Hamiltonian Monte Carlo [31, 32] as implemented in Stan [54], which allows us to quantify the parameter uncertainties.

b. Non-parametric weighted stochastic block models

In our analysis, we employ a class of stochastic block models (SBMs) where weights are represented as edge covariates [27]. These are generative models for networks that, in addition to the adjacency matrix $\mathbf{A} = \{A_{ij}\}$, also have real or discrete edge covariates $\mathbf{x} = \{x_{ij}\}$. This formulation decouples the edge existence from the presence of a null weight, i.e., the non-existence of an edge is different from an edge with zero weight. In the migration network under study we have a binary, asymmetric adjacency matrix, with $A_{ij} = 1$ if there is at least one migration from location j to location i and $A_{ij} = 0$ otherwise, and on each existing edge we have one positive integer weight $x_{ij} \in \mathbb{N}^+$ representing the total number of relocation events from location j to location i . The underlying assumption of the SBM is that nodes are divided into B groups, with each node having a value $b_i \in \{0, \dots, B-1\}$ specifying its group membership. In addition

to the edge placement, the edge weights are also sampled according to the group membership of the source and target node. This means that both the edges \mathbf{A} and the edge weights \mathbf{x} are sampled from parametric distributions conditioned on the group memberships of the nodes, i.e.

$$P(\mathbf{A}, \mathbf{x} | \boldsymbol{\theta}, \boldsymbol{\gamma}, \mathbf{b}) = P(\mathbf{x} | \mathbf{A}, \boldsymbol{\gamma}, \mathbf{b}) P(\mathbf{A} | \boldsymbol{\theta}, \mathbf{b}) \quad (9)$$

with the weights being sampled conditioned on the existence of the edges,

$$P(\mathbf{x} | \mathbf{A}, \boldsymbol{\gamma}, \mathbf{b}) = \prod_{rs} P(x_{rs} | \gamma_{rs}) \quad (10)$$

where $x_{rs} = \{x_{ij} | A_{ij} > 0 \wedge (b_i, b_j) = (r, s)\}$ are the covariates between groups r and s , with γ_{rs} being the parameters controlling the sampling of the weights, specific to the group pair. The placement of the edges is independent of the edge covariates and controlled by the parameters $\boldsymbol{\theta}$.

Given the generative model presented above—with a specific choice for the edge placements and the weight distributions—the set of parameters $\boldsymbol{\theta}$ and $\boldsymbol{\gamma}$ could be estimated via maximum likelihood. Doing so would lead to overfitting as the likelihood would increase with the complexity of the model. A more principled way to proceed is to obtain the Bayesian posterior probability for the partitions \mathbf{b} , i.e.

$$P(\mathbf{b} | \mathbf{A}, \mathbf{x}) = \frac{P(\mathbf{A}, \mathbf{x} | \mathbf{b}) P(\mathbf{b})}{P(\mathbf{A}, \mathbf{x})}, \quad (11)$$

where the numerator is the marginal likelihood of the observed network and weights, integrated over the model parameters,

$$P(\mathbf{A}, \mathbf{x} | \mathbf{b}) = \sum_{\boldsymbol{\theta}} \int P(\mathbf{A}, \mathbf{x} | \boldsymbol{\theta}, \boldsymbol{\gamma}, \mathbf{b}) P(\boldsymbol{\theta}) P(\boldsymbol{\gamma}) d\boldsymbol{\gamma} = P(\mathbf{A} | \mathbf{b}) P(\mathbf{x} | \mathbf{A}, \mathbf{b}). \quad (12)$$

For the edge placement—i.e. corresponding to $P(\mathbf{A} | \mathbf{b}) P(\mathbf{b})$ —we use the nested microcanonical degree-corrected SBM described in Ref. [55]. The degree correction [56] of the model prescribes, in addition to the modular group structure, that the networks generated by the model possess a specific out- and in-degree sequence, $\mathbf{k} = \{k_i^+, k_i^-\}$. The edges are placed according to

$$P(\mathbf{A} | \boldsymbol{\theta} = \{\mathbf{e}, \mathbf{k}\}, \mathbf{b}) = \frac{\prod_i k_i^+! k_i^-! \prod_{rs} e_{rs}!}{\prod_r e_r^+! e_r^-! \prod_{ij} A_{ij}!} \quad (13)$$

where $\mathbf{e} = \{e_{rs}\}$ specifies the number of edges that are placed between groups. The nested nature of this model is given by considering, as part of the prior probabilities for the edge placements, a hierarchy of multigraphs. The groups in the observed network are considered themselves as nodes of a smaller multigraph that is also generated by the SBM, with its nodes put in their own groups, forming an even smaller multigraph, and so on recursively. This gives a nested hierarchy with L levels $\{\mathbf{b}^l\} = \{\{b_r^{(l)}\}_l\}$, where $b_r^{(l)} \in \{0, \dots, B_l - 1\}$ is the group membership of the group/node r at level $l \in \{0, \dots, L - 1\}$, with the boundary condition that at the topmost level there is only one group, $B_L = 1$. The adjacency of the multigraph at level l is

$$e_{rs}^l = \sum_{t,u} e_{tu}^{l-1} \delta_{b_t^{(l)}, r} \delta_{b_u^{(l)}, s} \quad (14)$$

with $e_{ij}^0 = A_{ij}$ as a boundary condition. This hierarchy of partitions allows for a multilevel description of the network data under study—describing in the migration network the mesoscopic structure of the migration flow at different geographical resolutions.

The marginal likelihood of the edge weights completes the nonparametric approach presented in Ref. [27]. This is obtained by integrating over the weight parameters $\boldsymbol{\gamma}$,

$$P(\mathbf{x} | \mathbf{A}, \mathbf{b}) = \int P(\mathbf{x} | \mathbf{A}, \boldsymbol{\gamma}, \mathbf{b}) P(\boldsymbol{\gamma}) d\boldsymbol{\gamma} = \prod_{rs} \int P(x_{rs} | \gamma_{rs}) P(\gamma_{rs}) d\gamma_{rs}. \quad (15)$$

This formulation of the model allows us to consider a variety of elementary choices for the terms appearing in Eq. (15), reflecting the nature of the covariates (e.g. continuous or discrete, signed or not, bounded or unbounded). Among the different formulations compatible with the characteristics of the covariates under study, we select the best model according to the choice that yields the smallest description length—the negative log-likelihood for models with discrete covariates—or by computing the posterior odds ratio for continuous models, as described in Refs. [27, 57]. For the networks of Austrian migrations, where edges weights correspond to relocation counts, i.e. $x_{ij} \in \mathbb{N}^+$, the two elementary choices are to consider a Poisson or a geometric distribution. The model with weights sampled from geometric distributions consistently provided a better fit (i.e. smaller description length) for the data under study, which is compatible with the underdispersion of Poisson formulations found previously in the literature [23].

Given a choice for the marginal likelihood in the numerator of Eq. (11), we find the best hierarchical partition of the network under study by employing the efficient agglomerative multilevel Markov chain Monte Carlo (MCMC) algorithm described in Refs. [55, 58] and further refining the results running the MCMC at null temperature. This procedure is performed for 10 different random initializations, where after running the agglomerative heuristic, we run the greedy MCMC for 3×10^4 sweeps. Out of these 10 states, we select the one yielding the lowest description length.

Acknowledgments

The authors acknowledge support from the project “MOMA: Multiscale network modeling of migration flows in Austria” funded by WWTF (Grant ID: 10.47379/ESS22032). The computational results have been achieved using the Austrian Scientific Computing (ASC) infrastructure. We also thank A. Malek and M. Czaika for fruitful discussion on this work.

References

- [1] D. G. Papademetriou and P. L. Martin, *The unsettled relationship: Labor migration and economic development*, 33 (Greenwood Publishing Group, 1991).
- [2] M. Czaika and C. Reinprecht, in *Introduction to migration studies: An interactive guide to the literatures on migration and diversity* (Springer International Publishing Cham, 2022) pp. 49–82.
- [3] P. Scholten, A. Pisarevskaya, and N. Levy, in *Introduction to Migration Studies: An Interactive Guide to the Literatures on Migration and Diversity* (Springer, 2022) pp. 3–24.
- [4] H. Barbosa, M. Barthelemy, G. Ghoshal, C. R. James, M. Lenormand, T. Louail, R. Menezes, J. J. Ramasco, F. Simini, and M. Tomasini, *Physics Reports* **734**, 1 (2018), human mobility: Models and applications.
- [5] D. Brockmann, L. Hufnagel, and T. Geisel, *Nature* **439**, 462 (2006).
- [6] M. C. Gonzalez, C. A. Hidalgo, and A.-L. Barabasi, *nature* **453**, 779 (2008).
- [7] C. Song, T. Koren, P. Wang, and A.-L. Barabási, *Nature physics* **6**, 818 (2010).
- [8] G. K. Zipf, *American Sociological Review* **11**, 677 (1946).
- [9] J. J. Lewer and H. Van den Berg, *Economics letters* **99**, 164 (2008).
- [10] R. Prieto Curiel, L. Pappalardo, L. Gabrielli, and S. R. Bishop, *PloS one* **13**, e0199892 (2018).
- [11] O. Cabanas-Tirapu, L. Danús, E. Moro, M. Sales-Pardo, and R. Guimerà, *Nature Communications* **16**, 1336 (2025).
- [12] M. Mazzoli, A. Molas, A. Bassolas, M. Lenormand, P. Colet, and J. J. Ramasco, *Nature communications* **10**, 3895 (2019).
- [13] O.-H. Kwon, I. Hong, W.-S. Jung, and H.-H. Jo, *EPJ Data Science* **12**, 57 (2023).
- [14] Y. Liu, Z. Sui, C. Kang, and Y. Gao, *PloS one* **9**, e86026 (2014).
- [15] R. Li, S. Gao, A. Luo, Q. Yao, B. Chen, F. Shang, R. Jiang, and H. E. Stanley, *Physical Review E* **103**, 012312 (2021).

- [16] P. Expert, T. S. Evans, V. D. Blondel, and R. Lambiotte, [Proceedings of the National Academy of Sciences](#) **108**, 7663 (2011).
- [17] J. Poot, O. Alimi, M. P. Cameron, and D. C. Maré, *Investigaciones Regionales-Journal of Regional Research* , 63 (2016).
- [18] S. A. Stouffer, [American Sociological Review](#) **5**, 845 (1940).
- [19] S. Akwawua and J. Pooler, in *Geography Research Forum* (Ben-Gurion University of the Negev Press, 2000) pp. 33–51.
- [20] F. Simini, M. C. González, A. Maritan, and A.-L. Barabási, [Nature](#) **484**, 96 (2012).
- [21] M. Lenormand, A. Bassolas, and J. J. Ramasco, *Journal of Transport Geography* **51**, 158 (2016).
- [22] Y. Yang, C. Herrera, N. Eagle, and M. C. González, *Scientific reports* **4**, 5662 (2014).
- [23] M. Burger, F. Van Oort, and G.-J. Linders, [Spatial economic analysis](#) **4**, 167 (2009).
- [24] A. P. Masucci, J. Serras, A. Johansson, and M. Batty, *Physical Review E—Statistical, Nonlinear, and Soft Matter Physics* **88**, 022812 (2013).
- [25] R. M. Beyer, J. Schewe, and H. Lotze-Campen, *Humanities and Social Sciences Communications* **9**, 1 (2022).
- [26] T. P. Peixoto, in *Advances in Network Clustering and Blockmodeling* (John Wiley & Sons, Ltd, 2019) pp. 289–332, [arXiv:1705.10225](#) .
- [27] T. P. Peixoto, [Physical Review E](#) **97**, 012306 (2018).
- [28] P. D. Grünwald, *The Minimum Description Length Principle* (The MIT Press, Cambridge, MA, 2007).
- [29] J. Rissanen, *Information and Complexity in Statistical Modeling*, 1st ed. (Springer, New York, 2010).
- [30] T. P. Peixoto, [Physical Review X](#) **4**, 011047 (2014), [arXiv:1310.4377](#) .
- [31] M. J. Betancourt and M. Girolami, “Hamiltonian monte carlo for hierarchical models,” (2013), [arXiv:1312.0906 \[stat.ME\]](#) .
- [32] A. Gelman, J. B. Carlin, H. S. Stern, D. B. Dunson, A. Vehtari, and D. B. Rubin, “Bayesian data analysis,” (Chapman and Hall/CRC, 2013) Chap. 12.
- [33] T. P. Peixoto, [Elements in the Structure and Dynamics of Complex Networks](#) (2023), [10.1017/9781009118897](#), [arXiv:2112.00183](#) .
- [34] L. Zhang and T. P. Peixoto, [Physical Review Research](#) **2**, 043271 (2020), [arXiv:2006.14493](#) .
- [35] D. Holten, [IEEE Transactions on Visualization and Computer Graphics](#) **12**, 741 (2006).
- [36] T. P. Peixoto, [Physical Review X](#) **11**, 021003 (2021), [arXiv:2005.13977](#) .
- [37] Available at <https://data.statistik.gv.at/>.
- [38] C. Ratti, S. Sobolevsky, F. Calabrese, C. Andris, J. Reades, M. Martino, R. Claxton, and S. H. Strogatz, *PloS one* **5**, e14248 (2010).
- [39] M. Menyhért, E. Bokányi, R. Corten, E. M. Heemskerk, Y. Kazmina, and F. W. Takes, *EPJ Data Science* **14**, 8 (2025).
- [40] J. Yin, S. , Aiman, Y. , Dandong, and S. and Wang, [International Journal of Geographical Information Science](#) **31**, 1293 (2017).
- [41] C. Thiemann, F. Theis, D. Grady, R. Brune, and D. Brockmann, [PLOS ONE](#) **5**, e15422 (2010).
- [42] A. De Montis, S. Caschili, and A. Chessa, *The European Physical Journal Special Topics* **215**, 75 (2013).
- [43] Y. Wei and X. Zhao, [IEEE Access](#) **12**, 159635 (2024).
- [44] G. Pintér and B. Lengyel, “Quantifying Barriers of Urban Mobility,” (2024), [arXiv:2312.11343 \[physics\]](#) .
- [45] D. Pitoski, T. J. Lampoltshammer, and P. Parycek, [Digital Government: Research and Practice](#) **2**, 25:1 (2021).
- [46] D. Pitoski, T. J. Lampoltshammer, and P. Parycek, [Computational Social Networks](#) **8**, 1 (2021).
- [47] F. Gürsoy and B. Badur, [Social Network Analysis and Mining](#) **12**, 150 (2022).

- [48] A. Sarra, D. D’Ingiullo, A. Evangelista, E. Nissi, D. Quaglione, and T. Di Battista, [Socio-Economic Planning Sciences](#) **100**, 102225 (2025).
- [49] J. Jeong, [Environment and Planning B: Urban Analytics and City Science](#) **51**, 1227 (2024).
- [50] “ÖNB-ALEX - Reichsgesetzblatt 1849-1918,” .
- [51] Z. Xu, [Papers in Regional Science](#) **97**, 785 (2018).
- [52] R. C. d. Carvalho and E. Charles-Edwards, [Population, Space and Place](#) **26**, e2332 (2020).
- [53] R. Flowerdew and M. Aitkin, [Journal of regional science](#) **22** (1982), <https://doi.org/10.1111/j.1467-9787.1982.tb00744.x>.
- [54] B. Carpenter, A. Gelman, M. D. Hoffman, D. Lee, B. Goodrich, M. Betancourt, M. Brubaker, J. Guo, P. Li, and A. Riddell, [Journal of Statistical Software](#) **76**, 1 (2017).
- [55] T. P. Peixoto, [Physical Review X](#) **4** (2014), 10.1103/physrevx.4.011047.
- [56] B. Karrer and M. E. J. Newman, [Physical Review E](#) **83**, 016107 (2011).
- [57] T. P. Peixoto, [Phys. Rev. E](#) **95**, 012317 (2017).
- [58] T. P. Peixoto, [Phys. Rev. E](#) **89**, 012804 (2014).

Results on binary network

In Fig. 9 we show the results equivalent to Fig. 4, but considering only a binarized version of the network, characterized by the adjacency matrix

$$A_{ij} = \begin{cases} 1, & \text{if } x_{ij} > 0 \\ 0, & \text{otherwise.} \end{cases} \quad (16)$$

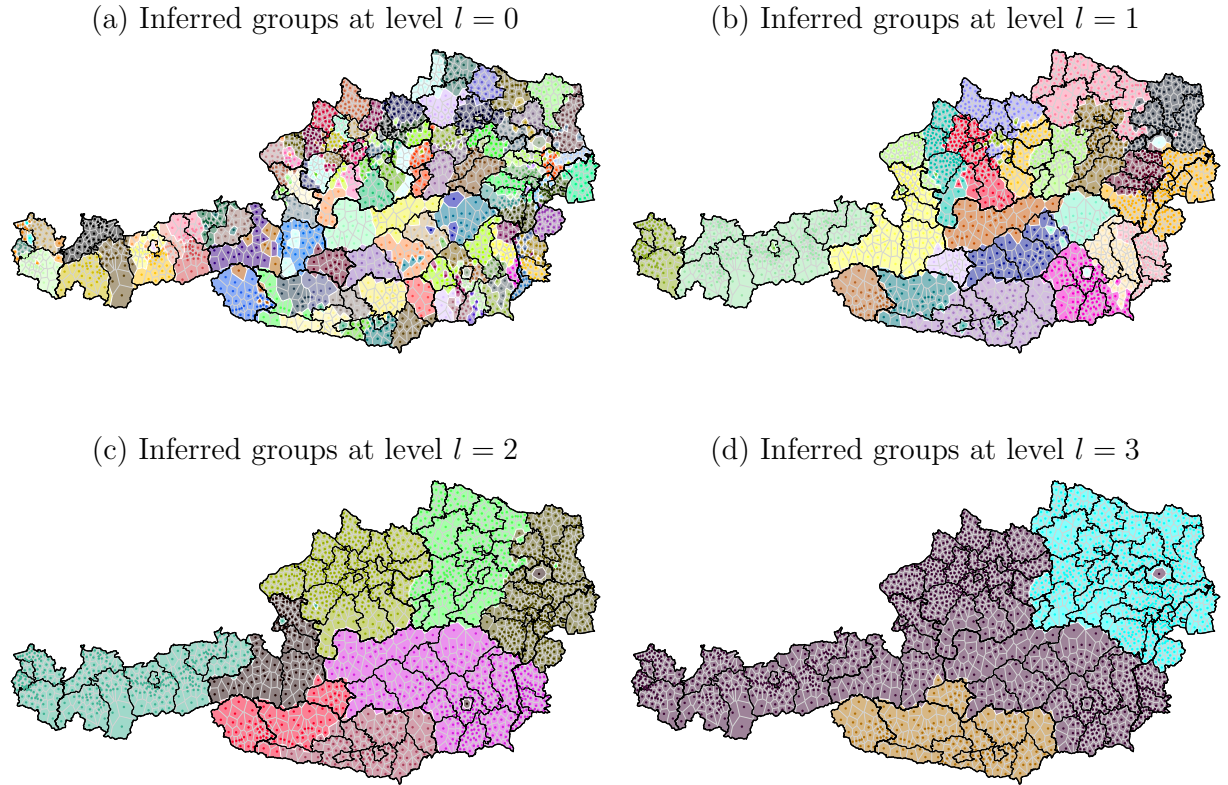


Figure 9: Inferred groups with the SBM for 2013, considering the binarized network, for different hierarchical levels l . Thick black lines indicate federal states boundaries, thin black lines denote districts borders.